Nerve growth factor-targeted molecular theranostics based on molybdenum disulfide nanosheet coated gold nanorods (MoS_2-AuNR) for osteoarthritis pain

Man Ting Au*, Jingyu Shi*, Yadi Fan, Junguo Ni, Chunyi Wen#, Mo Yang#

Department of Biomedical Engineering, Faculty of Engineering, Hong Kong Polytechnic University, Hong Kong

*: Equal contribution
#: Correspondence

Man Ting Au 15903037r@connect.polyu.hk
Jingyu Shi shijingyu.s@gmail.com
Yadi Fan yadi0731.fan@connect.polyu.hk
Junguo Ni jun-guo.ni@connect.polyu.hk
Chunyi Wem chunyi.wen@polyu.edu.hk
Mo Yang mo.yang@polyu.edu.hk

Corresponding authors:

Dr. Chunyi Wen
Department of Biomedical Engineering,
Faculty of Engineering,
The Hong Kong Polytechnic University, Hong Kong
E-mail: chunyi.wen@polyu.edu.hk

Prof. Mo Yang
Department of Biomedical Engineering,
Faculty of Engineering,
The Hong Kong Polytechnic University, Hong Kong
E-mail: mo.yang@polyu.edu.hk

ABSTRACT

Osteoarthritis (OA) is a leading cause of chronic pain in the elderly worldwide. Current diagnosis and therapy for OA pain are non-specific and inefficient with significant adverse effects. Here, we design a theranostic nanoprobe based on molybdenum disulphide (MoS_2) nanosheet-coated gold nanorods (MoS_2-AuNR) targeting never growth factor (NGF), a key player in OA pain sensation, for photoacoustic pain imaging and near-infrared (NIR) imaging-guided photothermal therapy in a surgical OA murine model. MoS_2 coating significantly improves the photoacoustic and photothermal performance of AuNR. Functionalization of MoS_2-AuNR nanoprobes by conjugating with NGF antibody enables active targeting on painful OA knees. Photoacoustic signal intensity reflected by probes accumulated in OA knee correlates with the severity of mechanical allodynia and near-infrared excited photothermal therapy mitigates mechanical allodynia in both subacute and chronic phase of OA. This molecular theranostic approach enables us to specifically localize and efficiently block peripheral OA pain transmission.

KEYWORDS: molybdenum disulfide, gold nanorods, osteoarthritis, nerve growth factor, theranostics, pain relief

Osteoarthritis (OA) represents one of the most common painful conditions in the life of a human. It has caused heavy healthcare and socioeconomic burden.[1] The pathophysiology of OA pain is a mixed picture involving both nociceptive and neuropathic mechanisms at both peripheral and central level.[2] As a result, OA pain exhibits heterogeneous clinical presentations, which poses a huge challenge for clinical diagnosis and management.[3]

In current clinical practice, the diagnosis and treatment for OA pain are limited to subjective description such as visual analogue score, and non-specific pain relief using nonsteroidal anti-inflammatory drugs (NSAIDs).[4] With the advancement of imaging technologies, functional magnetic resonance imaging, *i.e.* blood oxygenation level-dependent imaging, has been employed to quantify central pain sensitization component in OA.[5, 6] However, it remains puzzling why patients with relatively less severe radiographic joint deformity preoperatively experience much more pain after total joint replacement surgery,[7] and joint pain persistently occurs in around 10~20% of OA patients after surgery.[8] Seeing the discordance between radiographic and symptomatic OA,[9, 10] there might exist unknown peripheral OA pain generators that are not resected during the surgery. It promotes an urgent need for the development of imaging-based evaluation tools to precisely localize and quantify the peripheral component of OA pain, which will potentially lead to a paradigm shift in current analgesic and surgical practice.[11]

Activation and sensitization of peripheral afferent nerve fibres is a key step in OA pain mechanism along its chronic course.[12] Nerve growth factor (NGF) is a secreted protein that is essential for the development and survival of neurons.[13] Mounting evidence points to a pivotal role of NGF in OA peripheral pain transmission in both humans and animals.[14, 15] Under mechanical or inflammatory stimuli, articular chondrocytes or synovial fibroblasts secret NGF to trigger pain sensation in OA joint.[16,17] Accumulation of NGF can be observed in human OA patients and OA

models *in vivo.*[16,18,19] In a widely used surgical destabilization of medial meniscus (DMM) mouse model of OA, the level of *Ngf* mRNA in arthritic joint tissues reached the peak immediately (day 3) and 4 months after surgery.[15] The binding of NGF to its receptor, Tropomyosin receptor kinase A (TrkA), leads to a rapid potentiation of transient receptor potential cation channel, subfamily V, member 1 (TRPV1) that triggers pain sensitization in primary afferent sensory neurons.[20] NGF also contributes to the arthritic joint pain hypersensitivity.[21, 22] Recently, it was reported that pain behaviour in OA knees tended to be more sensitive to intra-articular injection of NGF.[17] Blockade of NGF signalling *via* either soluble recombinant form of NGF receptor or selective TrkA inhibitor could effectively suppress the pain in various animal models of OA,[15,23] while NGF neutralizing antibody is also an emerging analgesic therapy for OA in clinical trial phase III.[24] In recent years, there is increasing use of nanoprobes (cationic nanoprobe) and biomarkers (inflammatory and non-inflammatory cytokines) on OA theranostics.[25-27] Therefore, NGF-targeting molecular imaging using nanoprobes for OA pain will enable us a better understanding of the origin of OA pain towards personalized analgesic therapy.

Photoacoustic imaging is a non-invasive hybrid imaging modality, which rapidly arouses great attention in clinical diagnostics due to the non-ionizing property, high spatial resolution and deep penetration depth compared with optical imaging.[28] Plasmonic nanoparticles such as gold nanostructures (10~200 nm) have been well investigated as potential photothermal agents and PA contrast agents due to their super optical properties and easy biofunctionalization.[29,30] Compared with round gold nanoparticles (AuNPs) with main optical absorption in the visible light, anisotropic gold nanorod (AuNR) is of high interest for NIR-excited PA imaging due to easy synthesis, tuneable absorbance spectrum and high absorption cross-section in the near-infrared (NIR) region from 650 to 900 nm.[31] However, poor photothermal stability of AuNR limits the

wide application of PA imaging in biological samples.[32] To improve the photothermal stability and enhance PA imaging signal, AuNR coating with other nanomaterials such as silica and reduced graphene oxide (rGO) with efficient thermal conductivity have been used to coat on AuNR surface to increase its photothermal stability.[31,32] However, silica has no photothermal absorption in the NIR region, which cannot enhance the photothermal performance of AuNR.[31] The rGO coating with high NIR light absorption could enhance the photothermal performance of AuNR. However, the hydrophobic property of rGO leads to poor water dispersibility of the formed rGO-AuNR, which may hamper its biological applications.[32] In the recent years, graphene-like two-dimensional (2D) layered nanomaterials, have attracted great attention due to the graphene-like atomic planar structure.[33] Among them, molybdenum disulfide (MoS_2) is of high interest due to its high stability, easy synthesis, and unique chemical, electronic and optical properties.[34] Especially, MoS_2 shows excellent biocompatibility and low cytotoxicity, which makes it suitable for biological applications.[35-37] Moreover, due to its high NIR absorbance and strongly negative surface charge, chemically exploited 2D MoS_2 nanosheets exhibit good NIR heating feature as well as good water dispersibility.[38] Such properties of MoS_2 potentiate itself as a superior contrast agent for PA imaging, [39] or hybridization with the other nanomaterials for theranostic purpose.[40,41]

Here, we designed an NGF-targeting PA molecular theranostic nanoprobe based on 2D molybdenum disulfide (MoS_2) nanosheets-coated gold nanorods (MoS_2-AuNR) for peripheral OA pain imaging and imaging-guided photothermal treatment in animals. NGF monoclonal antibody-conjugated nanoprobe (Anti-NGF-MoS_2-AuNR) demonstrated its active targeting capability on OA knee joint compared to intact knee under molecular PA imaging *in vivo*. Our results demonstrated that the intensity of photoacoustic signal in OA knee after tail-vein injection correlates with the severity of mechanical allodynia and histopathological evidence of

neurovascular invasion in arthritic joint tissues in a surgical OA mouse model. Moreover, anti-NGF-MoS_2-AuNR mediated photothermal therapy displayed significant pain relief in both subacute and chronic phase of OA.

RESULTS AND DISCUSSION

Design and synthesis of NGF-targeted theranostic nanoprobe

Neurovascular invasion with joint destruction contributes to peripheral pain sensation in OA (Figure 1a). The binding of nerve growth factor (NGF) on tropomyosin receptor kinase A (TrkA) could lead to pain sensation.[42] To prevent NGF binding to TrkA in peripheral pain sensation, we purposely designed a functionalized gold nanorod (AuNR) coated with MoS_2 and then conjugated with anti-NGF antibody (anti-NGF-MoS_2-AuNR) (Figures 1b). As shown *via* high-resolution transmission electron microscopy, we successfully synthesized MoS_2-AuNR with MoS_2 coating layer on the surface of AuNR (aspect ratio of 2.5, length=50 nm, width=20 nm) (Figure 1c). The overlapping of Mo and S elements with Au element in the TEM elemental images indicated the formation of MoS_2 layer on the surface of AuNR (Figure 1c). Differences in surface charges between AuNR, MoS_2-AuNR and anti-NGF-MoS_2-AuNR were confirmed by changes in zeta-potential, suggesting the successful formation of the conjugate (Figure 1d). The chemical properties of MoS_2-AuNR have also been further characterized *via* Raman spectroscopy and X-ray diffraction analysis (Figures 1e & S1). In Raman spectroscopy, MoS_2 showed characterization peaks at 380 cm^{-1} and 402 cm^{-1} as the E^1_{2g} and A_{1g} vibration modes, respectively. After interaction with AuNR, the A_{1g} peak of MoS_2 showed a red-shift of 1.86 cm^{-1} and an increase of A_{1g}/ E^1_{2g} peak ratio was also observed due to the interaction between the MoS_2 layer and AuNR. In addition to the physical and chemical properties, we examined the binding affinity of our anti-NGF-MoS_2-

AuNR nanocomplex by ELISA (Figure 1f). The binding of anti-NGF-MoS_2-AuNR complex was significantly enhanced with increasing concentration of NGF (Figure 1g).

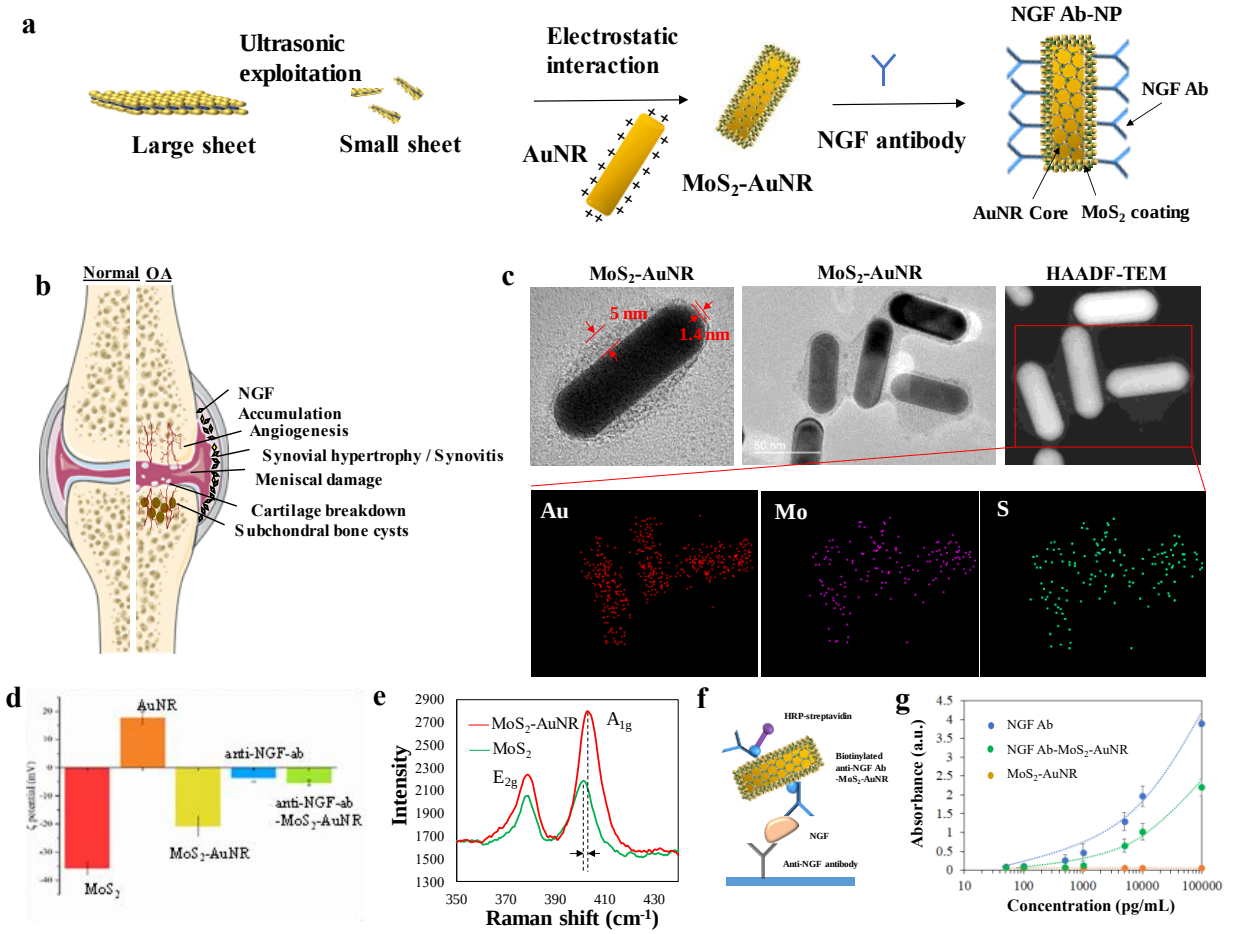

Figure 1 | Theranostic platform for pain imaging in knee osteoarthritis. a, Schematic diagram showing comparisons between normal and OA knee joint. **b,** Positively charged CTAB-AuNR interacts with negatively charged small MoS_2 nanosheet *via* electrostatic interaction to obtain MoS_2-nanosheet encapsulated AuNR (MoS_2-AuNR). Then anti-NGF antibody binds to MoS_2-AuNR *via* covalent interaction between MoS_2 nanosheet with sulfur vacancies and free sulfhydryl groups of the antibody. Finally, an anti-NGF-mAbs-MoS_2-AuNPs nanocomplex was obtained.**c,** HR-TEM images of single, multiple and element mapping images of MoS_2-AuNR **d,** Zeta-potential of elements in anti-NGF-MoS_2-AuNR, showing successful attachment of NGF antibody on MoS_2-AuNR **e,** Raman spectroscopy diagram of MoS_2-AuNR **f, g,** Binding affinity between anti-NGF-MoS_2-AuNR nanocomplex and NGF was assessed by **(f)** sandwich ELISA. **(g)** The absorbance at 450 nm was plotted against the increasing concentration of the antibody alone and the nanocomplex.

Enhanced biocompatibility and imaging performance of MoS_2-AuNR

High optical absorbance and high photothermal conversion efficiency of contrast agents in the NIR region are required to promote strong thermal expansion and to generate an enhanced PA signal.[28] Higher characteristic optical absorption peaks at 710 nm and 510 nm were achieved by coating MoS_2 on AuNR (Figure S2), while enhanced temperature under radiation was recorded in MoS_2-AuNR when compared to AuNR or MoS_2 alone (Figure S3). MoS_2-AuNR exhibits photothermal capabilities in a concentration- and power density-dependent manner (Figures 2a & S4), as well as in repeated heating and cooling cycles (Figure 2b). The photothermal conversion efficiency of MoS_2-AuNR was estimated at around 74.6% by average according to the photothermal heating/dissipation cycle (Figure S5).

PA imaging performance of MoS_2-AuNR was further investigated using a setup as shown in Figure S6. Finite element simulation showed a 4-fold increase in PA signals in MoS_2-AuNR than AuNR with a temporal laser pulse (Figure S7). This is further confirmed in the wavelength of the spectrum, with 4-fold higher PA amplitude in MoS_2-AuNR than AuNR at 710 nm (Figure 2c). Moreover, PA signal intensity of MoS_2-AuNR also increased in a dose-dependent manner from 50 to 400 μg/ml (Figures 2d & S8). Stability in morphology and PA intensities after long-term irradiation (710 nm, 20 Hz, 20 mJ/cm^2, < 10 ns pulse width) for 30 minutes make MoS_2-AuNR a good candidate for longitudinal imaging (Figure S9). Cellular uptake and haemolytic potential of this nanocomplex were evaluated before intravenous injection. Coated by the biocompatible MoS_2 layer, MoS_2-AuNR demonstrated lower cytotoxicity compared to AuNR alone (Figure S10). Strong TPEF signals were observed on MCF-7 cells incubated with a high concentration of 80 μg/mL MoS_2-AuNR up to 24 hours without causing any morphological alterations and cell damages (Figure S11). The hemolysis assay results also showed negligible

haemolysis (< 5%) of red blood cells upon AuNR, MoS_2 or MoS_2-AuNR treatment from 0-200 μg/ml, indicating excellent hemocapability of these nanoparticles (Figure 2e). We then examined the *in-vivo* PA imaging performance of MoS_2-AuNR in 4-6 months old balb/c mice. AuNR and MoS_2-AuNR solutions were mixed with matrigel matrix (v/v =1:1, the final concentration of Au was 75 μg/mL) and subcutaneously injected to the back of a mouse to generate the tissue-mimicking phantoms for *in vivo* PA evaluation (Figure 2f). Pure matrigel matrix was used as stronger than bare AuNR at 710 nm for *in vivo* imaging (Figures 2g, h).

We then investigated the biodistribution of MoS_2-AuNR by measuring the PA signal intensity of major organs such as heart, liver, kidney and spleen *ex vivo* after intravenous injection of MoS_2-AuNR at the dose of 3.5 mg/kg in 4-6-month-old female mice. The representative PA images of major organs at different time points are shown in Figure 2i. We observed that MoS_2-AuNR accumulation reached the maximum in most organs in the initial 6h especially in liver and spleen, and particles were mostly cleared out from major organs after 7 days (Figure 2j). This finding was further supported by the inductively coupled plasma mass spectrometry (ICP-MS) analysis (Figure 2k).

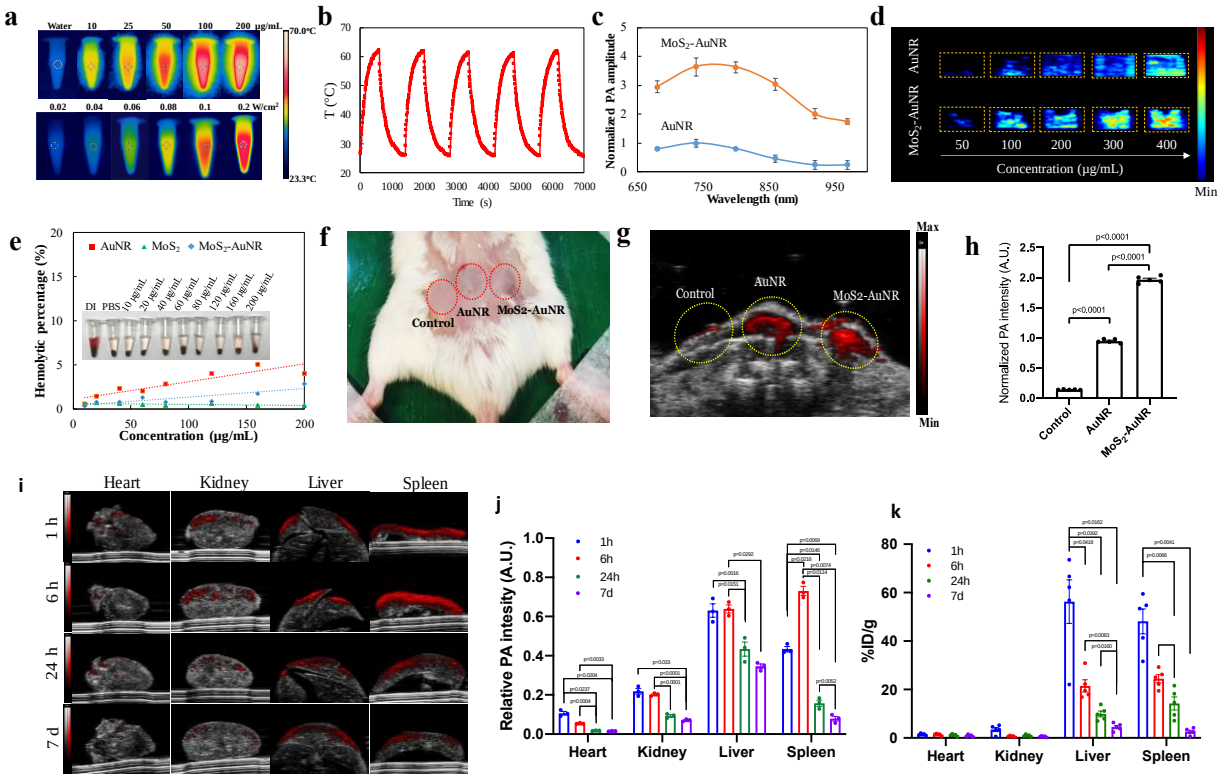

Figure 2 | Characterization and biocompatibility of MoS_2-AuNR. a, Thermal images of MoS_2-AuNR with increasing concentration (upper row) and increasing laser power (lower row) at 200 μg/mL **b,** Photothermal stability study of MoS_2-AuNR (200 μg/mL) under photothermal heating and natural cooling cycles. **c,** Normalized PA amplitude of AuNR and MoS_2-AuNR under different wavelengths **d,** PA signals for AuNR and MoS_2-AuNR showed a dose-dependent increase at 710 nm **e,** Percentages of hemolysis induced by AuNR, MoS_2 and MoS_2-AuNR at various concentrations. Inset image shows the direct observation of hemolysis by MoS_2-AuNR **f,** Subcutaneous injection of control (Matrigel), AuNR and MoS_2-AuNR into a mouse in prone position (n=5). **g,** US-PA overlay image obtained by *in vivo* PA imaging by LZ250 transducer at 710 nm. **h,** Quantitative analysis of PA signals from **(g)** showed an enhancement of signal with MoS_2-AuNR **i,** US-PA overlay images showing PA signals at 710 nm of *ex vivo* organs and tissues (heart, kidney, liver and spleen) from mice at 1h, 6h, 24h and 7 days post-i.v. injection of MoS_2-AuNR (n=3 each group). **j,** Semi-quantitative biodistribution of MoS_2-AuNR in mice determined by the average PA intensity of major organs. **k,** ICP-MS analysis reflecting the amount of gold element in MoS_2-AuNR in the excised tissues. A single intravenous injection of 3.5 mg/kg MoS_2-AuNR was given to the mice (n=20, 5 per group). Organs were collected after 1h, 6h, 24h or 7 days of injection. Statistical analyses were performed using ordinary one-way ANOVA with Tukey's post-hoc test.

Biodistribution of NGF-targeted nanoprobe for OA pain imaging

To confirm the successful delivery and active targeting effect of anti-NGF-MoS_2-AuNR to the inflamed joints, we carried out a time-dependent biodistribution of the nanocomplex after injection. A total of twenty 4-6 months balb/c mice were divided randomly into four groups (n=5) and sacrificed at different time points (1h, 6h, 24h and 7 days) after intravenous injection of 3.5 mg/kg anti-NGF-MoS_2-AuNR. *Ex vivo* US-PA overlay images of the organs showed accumulation of NPs mainly in liver, spleen and OA knee (Figure 3a). PA signals at 710 nm reached the maximum at 6h post-injection, while the signal diminished after 7 days (Figure 3b). In addition, we also quantified the gold deposition in the organs and inflamed knees using ICP-MS. Consistent with the observation from PA imaging, accumulation of NPs in OA knees reached the highest after 6 hours of injection (Figure 3c), suggesting 6 hours post-injection of NPs might be the optimal time for NGF-targeting therapy for OA pain relief. Histopathological H&E staining of major organs showed little difference between the saline control group and anti-NGF-MoS_2-AuNR group after 24 hours or 7 days of injection (Figure 3d). Hence, good biocompatibility of our nanoprobe *in vivo* affirmed its potential to be used in nanotherapy.

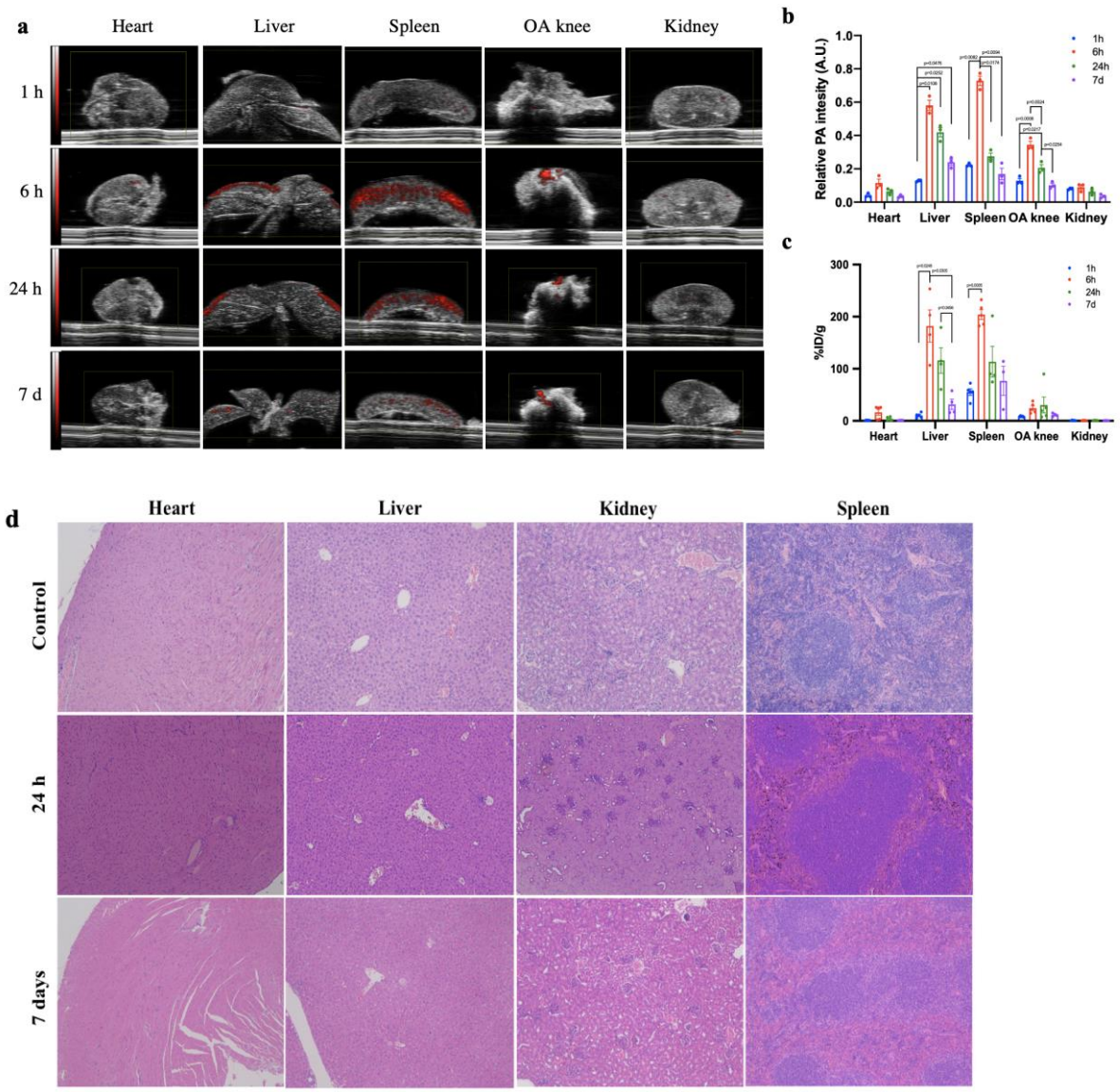

Figure 3 | Biodistribution and toxicity assessment of vital organs after anti-NGF-MoS_2-AuNR injection. a, US-PA overlay images showing signals at 710 nm of *ex vivo* organs and tissues (heart, liver, spleen, OA knee and kidney) at 1h, 6h, 24h and 7 days post-i.v. injection of anti-NGF-MoS_2-AuNR (n=3 each group). **b,** Semi-quantitative biodistribution of anti-NGF-MoS_2-AuNR in mice determined by the average PA intensity of major organs. **c,** ICP-MS analysis reflecting the amount of gold element in anti-NGF-MoS_2-AuNR in the excised tissues. A single intravenous injection of 3.5 mg/kg anti-NGF-MoS_2-AuNR was given to the mice after 1-month of surgery (n=20, 5 per group). Organs and knee joints were collected after 1h, 6h, 24h or 7 days of injection. **d,** Representative H&E staining of heart, liver, kidney and spleen after 24h of nanoprobe intravenous injection. Statistical analyses were performed using ordinary one-way ANOVA with Tukey's post-hoc test.

Non-invasive NGF-targeted pain imaging *in vivo*

In a well-received surgical destabilization of medial meniscus (DMM)-induced posttraumatic OA mouse model, the expression of nerve growth factor (NGF) and its receptor, tropomyosin receptor kinase A (TrkA) significantly increased in the synovium at 1-month and 4-month post-surgery (Figure 4a, 4b). Meanwhile, synovial blood flow transiently increased at 1-month post-surgery as visualized under Doppler sonography, and gradually resolved at 4-month after surgery (Figure 4c). Anti-NGF-MoS_2-AuNR was then deployed to localize NGF in this OA mouse model. Upon intravenous injection, our nanoprobes accumulated and could be visualized in the synovium of OA joints after 1 and 4-month of surgery under PA imaging at 710 nm (Figure 4d). No signal could be detected in unoperated intact knees, showing NPs only accumulate at the inflamed regions which are rich in NGF (Figures 4d, e). To differentiate between the true signal given by the nanoprobes and the signal from the haemoglobins which give information about oxygen saturation (sO_2) at 750/850 nm, we performed PA analysis at both 710 nm and 750/850nm.[35] Our PA imaging result showed sO_2 remain almost at the same level before and after NPs injection in OA knee (Figures 4f, g). This suggests that the difference in PA signal observed at 710 nm before and after surgery was not caused by the changes in surgery-induced sO_2 increase. The conjugated anti-NGF can actively target the inflammatory tissues in the OA joint.

Besides the increase of PA signals, histology of knee joints also suggested both passive and active targeting effect of anti-NGF-MoS_2-AuNR in OA synovium. H&E staining showed synovial membrane angiogenesis and degradation of articular cartilage in OA joints after 1-month and 4-month of DMM surgery respectively. We observed an increase in the number of blood vessels (as indicated by black arrows) in synovium after one month of surgery while the number reduced in late OA (4-month after surgery) (Figures 5a, b), which aligns well with the PA intensity.

The increase in permeability of the vessels as demonstrated by power Doppler imaging (Figure 4c) facilitates the passive movement of nanoparticles from the vessels to synovium by enhanced permeability and retention (EPR) effect. Nanoparticles (indicated by red rectangles) were observed near blood vessels, showing accumulation of NPs in inflamed tissue rich in NGF (Figure 5b). Moreover, no fibrosis or damaged tissues were observed in surrounding normal tissues, demonstrating good targeting effect of NIR laser treatment on NGF-positive tissues and the heat from the laser did not cause any adverse effect to other tissues at the joint (Figure 5b).

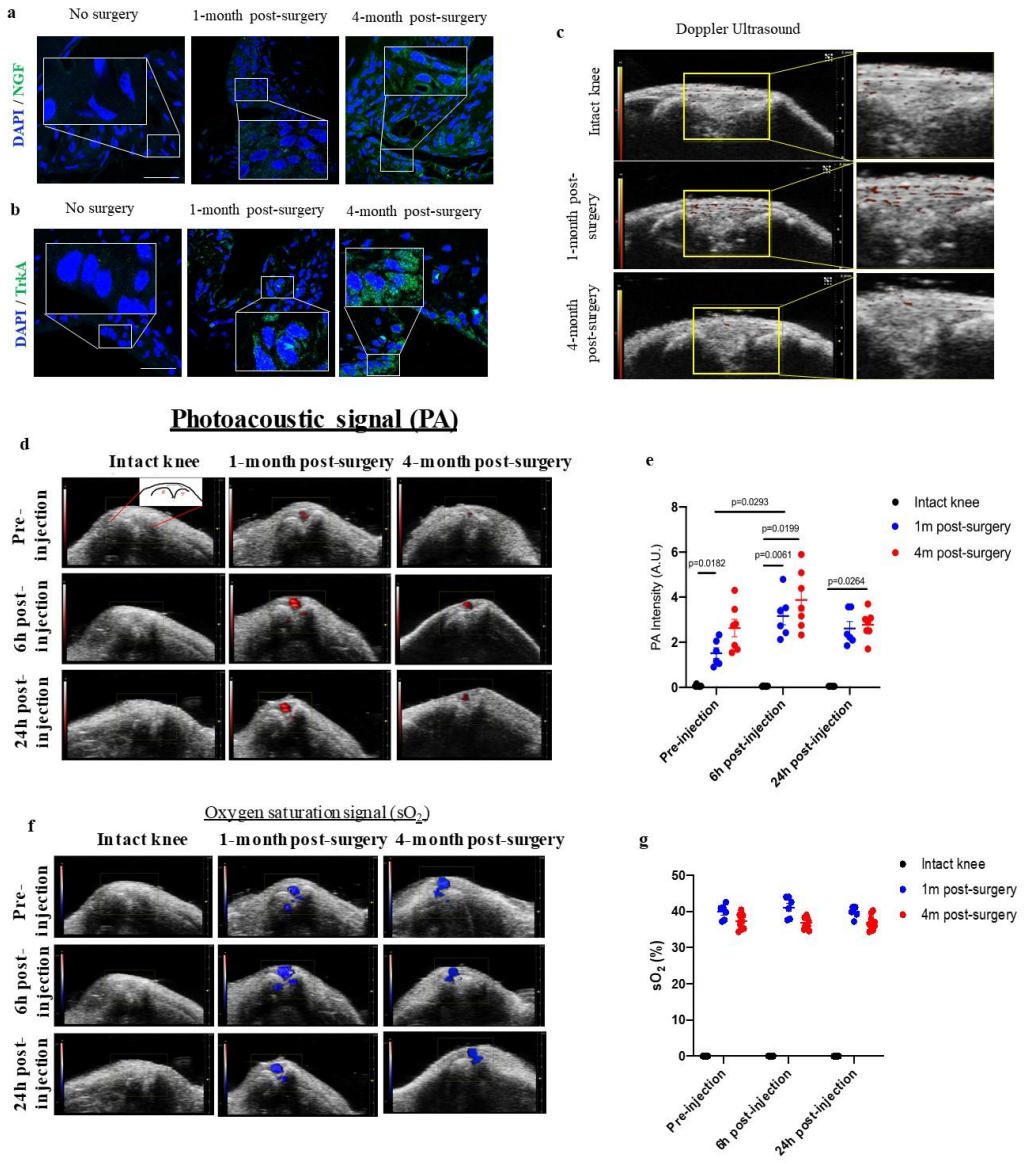

Figure 4 | Targeting effect of anti-NGF-MoS_2-AuNR on OA knee. a, NGF (green) and **b,** TrkA (green) expression were analysed by immunofluorescence staining, DAPI was used for nuclear counterstaining. Inset magnifications show a close-up view of synoviocytes in synovium. Scale bars, 25 μm. (n=6-7 independent biological samples for each group) **c,** Images of functional synovial vessels by power doppler (PD) ultrasonography. PD signals (red) reflect the flow rate of blood in blood vessels. Respective magnified images are shown on the right. (n=6-7). **d**, Representative *in vivo* US-PA overlay images of intact knees and surgery knees from mice after 1-month (n=6) and 4-month (n=10) of surgery at different time points (pre-i.v. injection, 6 hours and 24 hours post-i.v. injection of anti-NGF-MoS_2-AuNR). **e,** Quantitative PA intensities from **(d)** are shown with mean ± S.E.M. Each data point represents the signal from one knee. **f,** Representative US-PA overlay images showing oxygen saturation at wavelength 750/850 nm in synovial blood before and after injection in intact and OA knees. **g,** PA intensities from **(f)** are shown with mean ± S.E.M., with each data point represents signal from one knee.

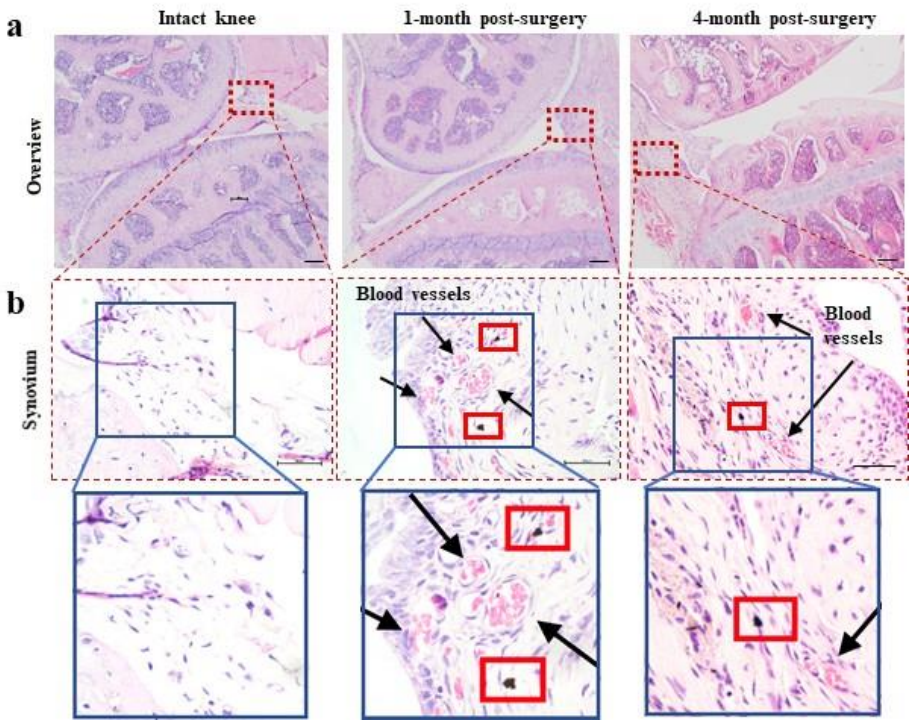

Figure 5 | Histology of knee joints indicating the targeting effects. a, Bright-field images of 5-μm slices of knee joints from control and OA mice stained with haematoxylin and eosin (H&E). **b,** Enlarged images of synovium showed in dotted rectangles of the **(a)** overview images. Black arrows indicate the presence of blood vessels. Scale bars, e, 100 μm; f, 50 μm. Statistical analyses were performed using ordinary one-way ANOVA with Tukey's post-hoc test or Kruskal–Wallis test with Dunn's multiple comparison test (non-normal distribution), when deemed appropriate.

Analgesic effect of NGF-targeted therapy in early OA

To determine the optimal concentration of MoS_2-AuNR intravenously injected into animals, a concentration screening test was peformed. Our results indicated concentration over 7.0 mg/kg will cause more than 5% haemolysis (Figure S12). We further measured the temperature of OA knees with NIR irradiation in mice injected with 1.75, 3.5 and 7 mg/kg. Low concentration at 1.75 mg/kg could not provide satisfactory hyperthermia treatment effect, while the middle and high dose provided similar increase in temperature (Figure S13). Therefore, the final concentration we used in our study was 3.5mg/kg. We successfully demonstrated the analgesic effect of our NGF-targeted photothermal therapy in early OA in a mouse model. Longitudinal nociception and motor coordination of the animals were monitored before and after surgery and NIR laser treatment (Figure 6a). Unoperated contralateral knees were used as the control for the OA knees. IR thermographs showed an increase in temperature on OA knees after injection of nanoprobes upon irradiation by an 808 nm laser with an output power of 0.2 W/cm^2 for 10 minutes (Figures 6b, c), while there was no obvious temperature change on intact knees. This again confirms the targeting effect on inflamed tissues of our anti-NGF-MoS_2-AuNR nanoprobes. To evaluate the long-term retention capability of our nanoprobes in OA knee, the temperature on the OA knee after 10 minutes of laser treatment was measured at different time points during 10 days post-injection. The results showed that the relative temperature increase on OA knee after laser treatment peaked at 6h post-injection and a slight drop in mean temperature was observed one day after injection. Temperature increase remained at a moderately high level even after 2 days of injection, then gradually decreased back to zero (Figure S14). This suggests the probes were completely cleared out and could not provide photothermal effect to the inflamed joint after 10 days of injection. We assessed the nociceptive tolerance of the animals on both the intact and OA legs before and after

NIR laser therapy. Surgery-induced hypersensitivity was observed in OA legs as shown by a large reduction in paw withdrawal threshold in von Frey test. The threshold remained low until we intravenously injected our nanoprobes and performed NIR therapy on the knee joints. Improvement in pain sensitization was reflected by an increase in paw withdrawal threshold in OA limbs upon laser treatment at 6h and 24h of post-injection (Figure 6d), showing successful pain-relief on our OA mouse model. In addition to pain relief, we also showed an improvement in motor balance of OA mice after NGF-targeted photothermal therapy (Figure 5e). In rotarod test which assesses the motor coordination of the animals, healthy mice could stay a longer time on an accelerating rod compared to OA mice. After treatment, the performance of the animals improved significantly after 6h and 24h of post-injection (Figure 6e). In a long-term efficacy study up to 10 days of post-injection, animals performed best after 2 days of injection. Analgesic effect brought by nanoprobe-based photothermal treatment lasted until 4 days after injection, while some animals still had a high paw withdrawal threshold after 4 days of injection and some animals lost analgesic effect. Our data indicated that complete loss of analgesic effect happened after 7 days of injection, when most of the nanoparticles were cleared out (Figure S15a). Similar trend was also found during the long-term von Frey test that the effect of the treatment could last for at least 4 days and the beneficial effect was lost only after 7 days of injection (Figure S15b). The therapy effect of our nanoprobe was also compared to indomethacin, one common nonsteroidal anti-inflammatory drug (NSAID) for acute pain treatment.. Here, indomethacin was administered once intraperitoneally (2.5 mg/kg) for comparison with the nanoprobe treatment group up to 7 days after injection. Indomethacin treatment group could improve motor balance and nociceptive tolerance at 6 h of injection and then quickly lost the therapy effect after 24 h of injection. Compared with indomethacin treatment group, the nanoprobe treatment group obviously had higher and longer

therapy effect up to 4 days. This again demonstrated the long-lasting effect of our active-targeting nanoprobe on OA knees. Expression of NGF reduced in OA synovium after NIR therapy, while there was no significant change in TrkA expression (Figure 6f, g). This imaging-guided nanotherapy successfully reduces the level of pain by preventing NGF from binding to its receptor without damaging TrkA, therefore, blocking the pain response pathway. It further affirms the targeting effect of our nanoprobes on the NGF-rich tissues.

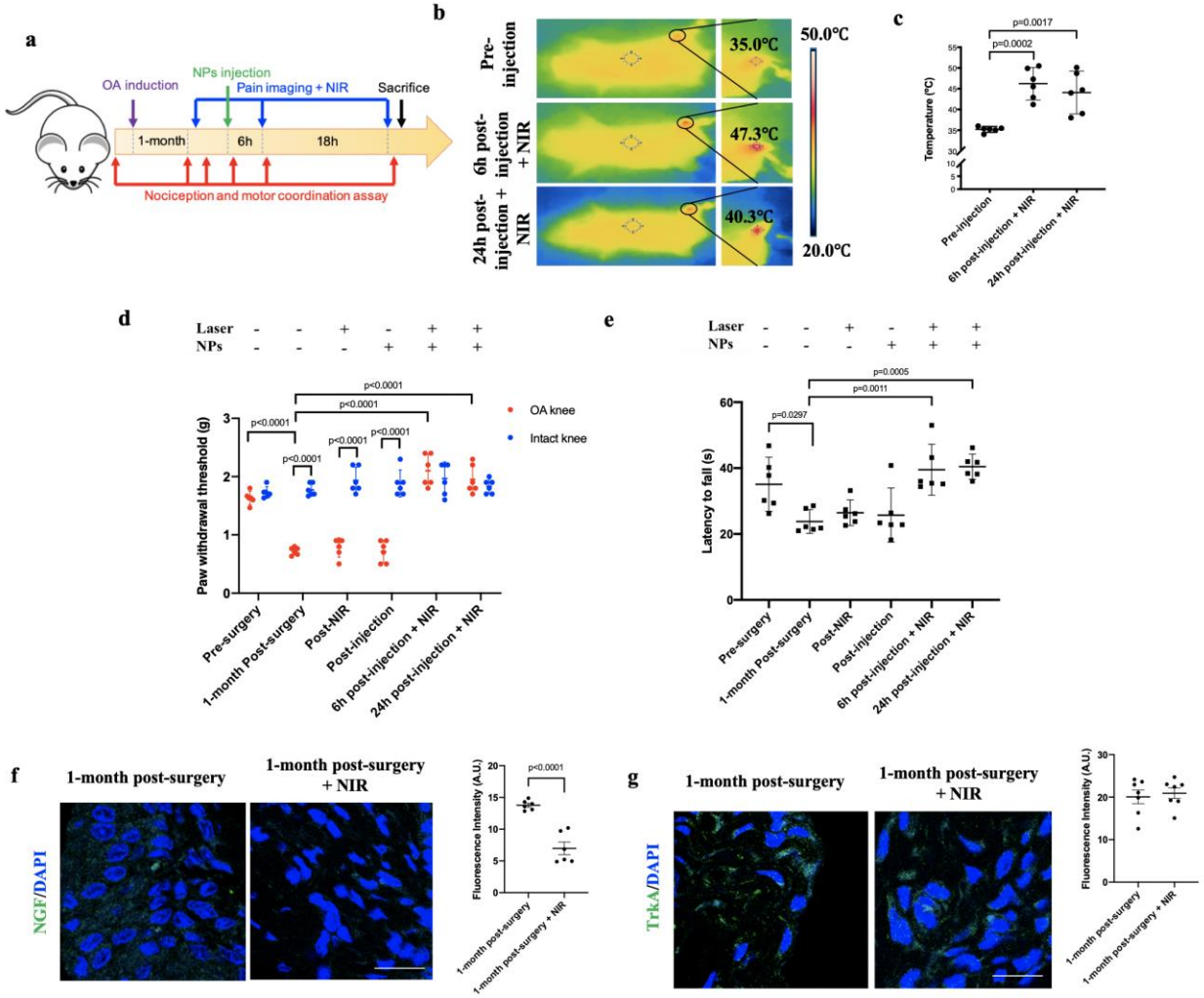

Figure 6 | Therapeutic effect of nanoprobe-guided laser treatment in early OA. a, Schematic diagram of the experimental design to investigate the effect of the photothermal therapy on early OA. (n=6). **b,** IR thermographs showed an increase of temperature in OA knees after intravenous injection of anti-NGF-MoS_2-AuNR in 1-month post-surgery mice. Temperature of the knees was measured and the zoomed-in thermographs are shown on the right. **c,** Temperature of the OA knees before and 6h/24h after injection. **d,** Paw withdrawal threshold in response to mechanical stimuli in intact and OA knees was evaluated by von Frey filament test after 1-month of surgery. **e,** Motor coordination of mice after 1-month of surgery was assessed by latency to fall using rotarod test. **f, g,** Representative images and quantification of immunofluorescence staining of **(f)** NGF and **(g)** TrkA on synovium of knee joints 1-month after surgery with and without NIR treatment. Scale bar, 25 μm. Data are shown with mean ± S.E.M. Each data point represents data from one animal. Two-way ANOVA with Sidak's multiple comparisons test was used for statistical analysis.

Analgesic effect of NGF-targeted therapy in advanced OA

To investigate the effect of the nanotherapy in advanced OA, we again examined the changes in tactile sensitivity and motor coordination of the animals after 4-month of surgery (Figure 7a). Similarly, the temperature of OA knee joints increased more than the contralateral sham-operated knees and reached a peak at 6 hours post-injection (Figure 7b). Lower degree of vascularization (Fig. 4f) with lower doppler signal measured in Doppler ultrasonography (Figure 4c) in more severe OA may cause a smaller difference in temperature recorded before and after injection of nanoprobes in OA knees compared to that in early OA knees (Figure 7b, c). Similar to the observation in early OA, laser treatment after injection of anti-NGF-MoS_2-AuNR also reversed the hypersensitivity in advanced OA (Figure 6d). However, it could not improve the motor coordination of mice after 4-month of surgery (Figure 7e). By normalizing the PA intensity and paw withdrawal threshold after 6 hours of nanoprobe injection and NIR therapy in both early and late OA, we observed a strong negative correlation ($r = -0.7133$) between the two (Figure 6f). This showed an accumulation of NGF when the mice experienced a more painful feeling, allowing visualization of nociception in animals. Again, we observed a significant reduction of NGF expression while no obvious decrease of TrkA after photothermal therapy (Figure 7g, h). The photothermal pain medication mechanism can be explained by Figure 7i. The pain sensation is based on the conjugation of NGF and its receptor TrkA on endothelial cells and sensory nerve. Once anti-NGF-MoS_2-AuNR nanoprobes conjugate with NGF, NIR based photothermal local treatment will prevent binding of NGF to TrkA. NGF/TrkA peripheral pain sensation signalling pathway through dorsal root ganglion is then blocked, realizing pain relief effects.

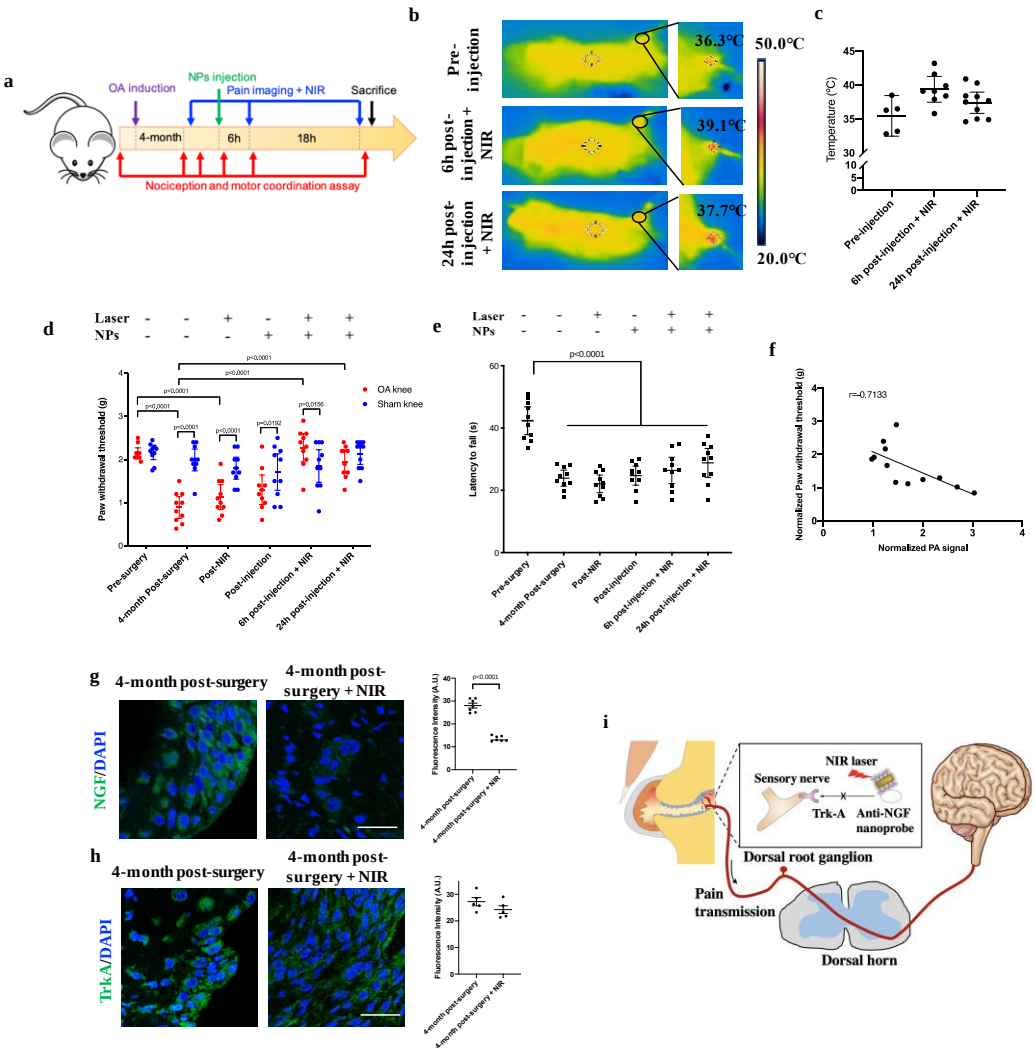

Figure 7 | Therapeutic effect of nanoprobe-guided laser treatment in late OA. a, Schematic diagram of the experimental design to investigate the effect of the photothermal therapy on late OA. (n=10). **b,** Thermographs of OA knees after 6h of anti-NGF-MoS_2-AuNR injection in 4-month post-surgery mice. Temperature of the knees was measured and the zoomed-in thermographs are shown on the right. **c,** Temperature of the OA knees before and 6h/24h after injection. **d,** Paw withdrawal threshold in response to mechanical stimuli in sham and OA knees were evaluated by von Frey filament test after 4-month of surgery. **e,** Motor coordination of mice after 4-month of DMM surgery was assessed by latency to fall using rotarod test. **f,** A negative correlation (r = -0.7133) was observed between normalized paw withdrawal threshold and normalized PA signal (n = 12 pairs) of mice 6-hour post-injection in 1- and 4-month post-surgery. Spearman's correlation coefficient r is shown on the graph. **g, h,** Representative images and quantification of immunofluorescence staining of **(g)** NGF and **(h)** TrkA on synovium of knee joints 4-month after surgery with and without NIR treatment. Scale bar, 25 μm. **i,** Schematic diagram showing NIR laser stops the binding of NGF to TrkA receptors, preventing transmission of pain signals from the periphery to spinal cord and brain. Data are shown with mean ± S.E.M. Each data point represents data from one animal. Two-way ANOVA with Sidak's multiple comparisons test was used for statistical analysis.

CONCLUSION

In conclusion, we developed an imaging-guided nanoparticle-based OA diagnosis and treatment method targeting NGF in synovium of the joint. The surface coating of MoS_2 on AuNR could simultaneously enhance the photothermal conversion efficiency and reduce the gold/water interfacial thermal resistance, thus leading to a significantly higher PA imaging signal with enhanced photothermal stability compared with bare AuNR. Combining NGF antibody with our small size MoS_2-AuNR nanoprobe allows both active and passive targeting in the OA joint for targeted near-infrared (NIR) treatment. Our results showed pain alleviation and improvement of motor function in a post-traumatic OA mouse model using targeted laser treatment. This theranostic platform not only allows us to visualise and quantify but also to mitigate pain in OA joint. We demonstrated the feasibility and desirability of this system, which could possibly be translated into a broader spectrum of clinical application.

METHODS

Preparation of molybdenum disulfide modified gold nanosheet (MoS_2-AuNR)

To obtain small-sized MoS_2 nanosheets, MoS_2 solution (2 mg/mL) was sonicated in an ice bath for 4h, and then centrifuged at 8000 rpm for 15 min. The obtained supernatant was filtered through a 0.22 μm microporous membrane and stored at 4 °C for further usage. Next, MoS_2 modified AuNR was prepared by electrostatic interaction between positively charged AuNRs and negatively charged MoS_2. AuNR solution (600 μg/ml) was slowly added dropwise to MoS_2 solution (1:1, v/v) with gentle stirring. After incubating at room temperature overnight, the sample was centrifuged at 6000 rpm for 15 min to separate unbound MoS_2 nanosheets in the supernatant. The obtained precipitate was re-dispersed in deionized water and stored at 4 °C for further usage.

Preparation of *anti-NGF monoclonal antibody-conjugated MoS_2-AuNR (anti-NGF-MoS_2-AuNR)*

Five μL of anti-NGF mAbs solution (100 μg/mL) was added into MoS_2-AuNR solution and incubated overnight at 4 °C to produce anti-NGF mAbs-MoS_2-AuNR bioconjugates. The mAbs could bind to MoS_2-AuNR *via* covalent interaction between MoS_2 nanosheet with sulfur vacancies and free sulfhydryl groups of the antibody.[43] The obtained mixture was purified at 6000 rpm for 10 min and then re-suspended in phosphate-buffered saline (PBS) for further usage.

Measurement of *in vitro* photothermal effect

To study the concentration- and time-dependent photothermal effects, MoS_2-AuNRs at different concentrations (10, 25, 50, 100 and 200 μg/mL, 200 μL) were suspended in centrifuge tubes and irradiated by an 808 nm laser at an output power of 0.2 W cm^{-2} for 10 min, respectively. During

the irradiation, the temperature of the solutions was recorded every 100 seconds and the IR thermographs were collected at the end (600 s) using a FLIR C2 infrared camera, respectively. In the same manner, the time-dependent photothermal properties of AuNR and MoS_2 (at the same concentration of 200 μg/mL) were studied under an 808 nm laser (0.2 W/cm^2, 10 min), respectively. The power density- and time-dependent photothermal properties of MoS_2-AuNRs (200 μg/mL) were investigated with different power densities ranging from 0.02 to

***In vivo* evaluation of MoS_2-AuNR photoacoustic performance by subcutaneous injection**

The use of animals in this study was conducted according to the requirements of the Cap. 340 Animal (Control of Experiments) Ordinance and Regulations in Hong Kong. All the animal experiments were approved by Animal Subjects Ethics Sub-Committee (ASESC). To analyze the PA contrast performance *in vivo*, AuNRs and MoS_2-AuNRs at the same concentrations of gold (150 μg/mL) were respectively mixed with matrigel (BD Bioscience, CA, USA) at 1:1 (v/v) ratio in an ice bath. Each mixture (total volume 100 μL, final concentration of AuNR was 75 μg/mL) was then subcutaneously injected into the back of 12-week-old female Balb/C mice (n = 3). Subcutaneous injection of matrigel alone was used as the control group. After the injection, the tissue-mimicking phantom was successfully generated due to the fast solidification of the matrigel when the temperature increased. All the samples were imaged simultaneously by the ultrasound micro-imaging system under 710 nm excitation. The laser condition and parameters of PA measurements were the same as *in vitro* evaluation. The data of each sample was collected with the same area of ROIs in PA images (1.66 mm^2) to ensure a fair assessment of *in vivo* results.

In vitro binding affinity test of anti-NGF-MoS_2-AuNR complex

The biological affinity of anti-NGF mAbs conjugated MoS_2-AuNR complex to NGF mAbs was evaluated by ELISA. Anti-NGF antibody was firstly coated in a 96-well plate. 100 μL of NGF (100 ng/mL) was then added to appropriate wells, incubating for 2.5h at room temperature with gentle shaking. After rinsing with prepared wash buffer five times, 100 μL of biotinylated anti-NGF mAbs-MoS_2-AuNRat different concentrations, ranging from 0.05 to 100 ng/mL, were respectively added into each well and incubated for 1 h with gentle shaking. The usages of biotinylated anti-NGF mAbs and MoS_2-AuNR were acted as positive and negative control groups, respectively. After the thoroughly washing step, streptavidin solution (100 μL) was added to each well and incubated for 45 min at room temperature. Next, 100 μL of TMB one-step substrate reagent was added into each well and incubated for another 30 mins in dark. Last, 50 μL of stop solution was added. The absorbance was measured immediately at 450 nm with a microplate reader. Each group has three replicates.

Animals and DMM Surgery

Institutional Animal Subjects Ethics Sub-Committee (ASESC) approved all the experiments listed below (ASESC Case 15-16/17-BME-R-HMRF). Animals were raised in constant temperature at 25°C, with 12/12 light-dark cycle and supplied with food and water ad libitum. To generate a post-traumatic OA model, destabilization of medial meniscus (DMM) was performed when the mice reached 4-week according to established protocol.[44] Briefly, the mice were anesthetized by intraperitoneal injection of an anaesthetic cocktail [ketamine (100mg/mL): Xylazine (20mg/mL): saline = 1:0.5:8.5]. Knee joints were opened, and the medial meniscus was cut. No surgery or sham

operation was performed on the contralateral knees in 1-month and 4-month post-surgery group respectively.

In vivo experimental design

Freshly prepared MoS_2-Gold nanorod conjugated with anti-NGF antibody (anti-NGF-MoS2-AuNR) was injected intravenously 80 µg/mL from the tail 1-month and 4-month post-surgery. Photoacoustic (PA) imaging was used to delineate the distribution of the nanoparticles *in vivo*. OA knees were exposed to near-infrared (NIR) therapy for 10 minutes under the photothermal camera. NIR treatment was carried out 6 hours and 24 hours after injection of nanoparticles. Von Frey and rotarod tests were performed to assess the locomotive ability and balance of the animals respectively. Knee joints were harvested 24 hours after injection and immunohistochemical analysis was carried out.

High-frequency ultrasound, Photoacoustic and Power doppler imaging

Vevo2100 high-frequency Micro-Imaging System (VisualSonics, Toronto, Ontario, Canada) was used for *in vivo* ultrasound, power doppler and photoacoustic (PA) imaging of the mice knees according to previously reported.[45] Briefly, the animal was put into general anaesthesia by 1%-3% isoflurane inhalation. The heart rate and respiratory rate were monitored by attaching the extremities of the animals to the electrodes on the heating pad of 37°C. The legs were flexed to approximately 120°, the position was fixed using medical tapes. Coupling gel was applied to provide a clear visualization of the knee joint. LZ250 transducer with a broadband frequency of 13-24 MHz was placed parallelly to the limb to obtain a sagittal plane of the joint until a triangular region was observed to ensure consistency. PA signal was measured at 710nm. The **PA** acquisition

parameters are as follows: frequency: 21 MHz; power: 100%; PA gain: 30 dB; B-mode gain: 18 dB; focus depth: 6 mm; Line density: high; Persistence: off; Sensitivity: high; Dynamic range: 65 dB; Display map: G5; Brightness: 50; Contrast: 50. For **power doppler** acquisition parameters: Frequency: 40 MHz; Power: 100%; PRF (pulse repetition frequency): 1 kHz; Doppler gain: 35 dB; 2D Gain: 35 dB; Focus depth: 4.5 mm; Beam angle: 0 deg; Sensitivity: 5; Line density: full; Persistence: low; Dynamic range: 60 dB; Wall filter: high; Priority: 58%. For *ex vivo* organs imaging, the acquisition parameters were similar except the PA gain used was 35 dB. Two-hundred frames were captured and the average PA value was compared between groups. Same area of ROI for the same animal at different time points were compared.

Von Frey filament test

Nociceptive sensitization was evaluated by Electronic von Frey Anesthesiometer (IITC, USA), allowing detection of force values from 0-74 gram. A simplified up-down method was used as described by Bonin *et al*.[46] Basically, we started testing at middle filament #3, which corresponds to 1.3 gram, after optimization. Up-down rules were applied to select the next filament according to the literature. In brief, the mice were placed on an elevated mesh grid and were allowed to adapt to the environment before measurement. Filaments were applied to the midplantar surface of OA hind paw and the contralateral paw of the animal when four limbs were resting on the mesh. The force required to cause the withdrawal of hind paw was recorded after 5 presentations. The exact detected force was recorded by the anesthesiometer. Adjustment factor +/- 0.5 was added to the final reading from the LCD readout after 5 presentations.

Rotarod test

Motor coordination was assessed by performing a rotarod (Panlab, Harvard Apparatus) test (Movie S1). Mice were placed on the rotating lanes of 5 cm diameter and allowed to walk at a constant speed at 4 rpm for 30 seconds for adaptation. In this experiment, the rotation was set to accelerate from 4 to 40 rpm over 5 minutes. Latency to fall (in seconds) and rotation speed of the rod when the animals fell were recorded. Measurements were taken at different time points to assess the endurance and motor coordination of the animals before and after surgery and treatment.

Laser treatment and thermal imaging of mouse knee joint

The animal was fixed on a platform with extremities taped, with 1% - 3% isoflurane inhalation to maintain general anaesthesia. 808nm laser with an output power of 0.2 W cm^{-2} was applied on knee joints for 10 minutes. The tip of the laser probe was kept at a 1-cm distance to the irradiated skin, the temperature was measured and the thermographs were taken immediately after removal of the probe using a FLIR C2 infrared camera.

Biodistribution by Inductively coupled plasma mass spectrometry (ICP-MS)

Major organs, including heart, liver, spleen, kidney and knees, were harvested 1h, 6h, 24h and 7 days after MoS_2-AuNR injection and fixed with 10% formalin. The collected organs were then dried, weighed and digested by trace metal grade nitric acid (69%) solution at 130 °C. After that, all the samples were diluted to 25 ml and filtered through a 0.45 μm membrane. Then, ICP-MS was used to quantify the uptake amount of Au in different organs and joint tissue (Agilent 7500ce, Octopole reaction system, US). Each group has five mice as replicates.

Histology and immunohistochemistry

Samples were harvested at specific time points. Organs and knee joints were fixed in 4% paraformaldehyde (PFA) and joints were decalcified using 10% ethylenediaminetetraacetic acid (EDTA) at pH 7.4. The tissues were then dehydrated in an alcohol gradient and embedded in paraffin. Five-micrometre thick sections were used for Haematoxylin and Eosin (H&E) staining for histomorphological evaluation. For immunohistochemistry, the knee sections were incubated with primary antibodies of nerve growth factor (NGF, ab6199, Abcam) and Tropomyosin receptor kinase A (TrkA, ab216626, Abcam) overnight at 4°C, followed by visualization by fluorescence-conjugated secondary antibodies or diaminobenzidine (DAB). Leica TCS SPE Confocal Microscope and Nikon ECLIPSE 80i were used to capture the images.

Statistical analysis

All data were presented using mean $\pm$ SEM. For comparison of signal intensities, one-way analysis of variance (ANOVA) or Kruskal-Wallis test when deemed appropriate. Respective post-hoc tests were carried when overall significance was detected between groups. For parameters for behavioural tests between different time points, two-way ANOVA with Sidak's multiple comparisons test was used for statistical analysis. The level of significance was set at $p<0.05$. Statistical analysis and graphs were generated using SPSS 23.0 and Graphpad Prism 8.

ACKNOWLEDGEMENTS

This work was supported by Health and Medical Research Fund Scheme (01150087#, 16172691#), Research Grants Council of Hong Kong ECS (PolyU 251008/18M), GRF (PolyU 151061/20M) and NFSC/RGC schemes (N_PolyU520/20). The authors also thank the University Research Facility in Life Sciences (ULS) for providing equipment and technical support.

AUTHOR CONTRIBUTIONS

CYW and MY conceived and designed the experiments with MTA and JYS. MTA, JYS and YDF performed all experiments. All authors analysed and discussed the data. MTA, JYS, MY and CYW wrote the paper.

COMPETING INTERESTS

The authors declare no competing interests.

ADDITIONAL INFORMATION

Supplementary information is attached below for this manuscript. Authors can confirm that all relevant data are included in the paper and/ or its supplementary information files. Correspondence and requests for materials should be addressed to CYW.

REFERENCES

1. Puig-Junoy, J.; Ruiz Zamora, A., Socio-economic Costs of Osteoarthritis: a Systematic Review of Cost-of-illness Studies. *Semin. Arthritis Rheum.* **2015,** *44* (5), 531-541.
2. Malfait, A. M.; Schnitzer, T. J., Towards a Mechanism-based Approach to Pain Management in Osteoarthritis. *Nat Rev Rheumatol* **2013,** *9* (11), 654-64.
3. Hawker, G. A.; Stewart, L.; French, M. R.; Cibere, J.; Jordan, J. M.; March, L.; Suarez-Almazor, M.; Gooberman-Hill, R., Understanding the Pain Experience in Hip and Knee Osteoarthritis--an OARSI/OMERACT Initiative. *Osteoarthr. Cartil.* **2008,** *16* (4), 415-22.
4. Dieppe, P. A.; Lohmander, L. S., Pathogenesis and Management of Pain in Osteoarthritis. *Lancet* **2005,** *365* (9463), 965-73.
5. Yue, Y.; Collaku, A., Correlation of Pain Reduction with fMRI BOLD Response in Osteoarthritis Patients Treated with Paracetamol: Randomized, Double-Blind, Crossover Clinical Efficacy Study. *Pain Med* **2018,** *19* (2), 355-367.
6. Keszthelyi, D.; Aziz, Q.; Ruffle, J. K.; O'Daly, O.; Sanders, D.; Krause, K.; Williams, S. C. R.; Howard, M. A., Delineation between Different Components of Chronic Pain Using Dimension Reduction - an ASL fMRI Study in Hand Osteoarthritis. *Eur J Pain* **2018,** *22* (7), 1245-1254.
7. Valdes, A. M.; Doherty, S. A.; Zhang, W.; Muir, K. R.; Maciewicz, R. A.; Doherty, M., Inverse Relationship between Preoperative Radiographic Severity and Postoperative Pain in Patients with Osteoarthritis Who Have Undergone Total Joint Arthroplasty. *Semin. Arthritis Rheum.* **2012,** *41* (4), 568-75.
8. Hofmann, S.; Seitlinger, G.; Djahani, O.; Pietsch, M., The Painful Knee after TKA: a Diagnostic Algorithm for Failure Analysis. *Knee Surg. Sports Traumatol. Arthrosc.* **2011,** *19* (9), 1442-52.
9. Vargas, E. S. N. C. O.; Dos Anjos, R. L.; Santana, M. M. C.; Battistella, L. R.; Marcon Alfieri, F., Discordance between Radiographic Findings, Pain, and Superficial Temperature in Knee Osteoarthritis. *Reumatologia* **2020,** *58* (6), 375-380.
10. Bedson, J.; Croft, P. R., The Discordance between Clinical and Radiographic Knee Osteoarthritis: a Systematic Search and Summary of the Literature. *BMC. Musculoskelet. Disord.* **2008,** *9*.
11. Vincent, T. L., Peripheral Pain Mechanisms in Osteoarthritis. *Pain* **2020,** *161 Suppl 1*, S138-S146.
12. Miller, R. E.; Tran, P. B.; Obeidat, A. M.; Raghu, P.; Ishihara, S.; Miller, R. J.; Malfait, A. M., The Role of Peripheral Nociceptive Neurons in the Pathophysiology of Osteoarthritis Pain. *Curr. Osteoporos. Rep.* **2015,** *13* (5), 318-26.

13. Aloe, L.; Rocco, M. L.; Balzamino, B. O.; Micera, A., Nerve Growth Factor: Role in Growth, Differentiation and Controlling Cancer Cell Development. *J Exp Clin Cancer Res* **2016,** *35* (1), 116.
14. Aloe, L.; Tuveri, M. A.; Carcassi, U.; Levi-Montalcini, R., Nerve Growth Factor in the Synovial Fluid of Patients with Chronic Arthritis. *Arthritis Rheum* **1992,** *35* (3), 351-5.
15. McNamee, K. E.; Burleigh, A.; Gompels, L. L.; Feldmann, M.; Allen, S. J.; Williams, R. O.; Dawbarn, D.; Vincent, T. L.; Inglis, J. J., Treatment of Murine Osteoarthritis with TrkAd5 Reveals a Pivotal Role for Nerve Growth Factor in Non-inflammatory Joint Pain. *Pain* **2010,** *149* (2), 386-92.
16. Pecchi, E.; Priam, S.; Gosset, M.; Pigenet, A.; Sudre, L.; Laiguillon, M. C.; Berenbaum, F.; Houard, X., Induction of Nerve Growth Factor Expression and Release by Mechanical and Inflammatory Stimuli in Chondrocytes: Possible Involvement in Osteoarthritis Pain. *Arthritis Res. Ther.* **2014,** *16* (1), R16.
17. Ashraf, S.; Mapp, P. I.; Burston, J.; Bennett, A. J.; Chapman, V.; Walsh, D. A., Augmented Pain Behavioural Responses to Intra-articular Injection of Nerve Growth Factor in Two Animal Models of Osteoarthritis. *Ann Rheum Dis* **2013**.
18. Iannone, F.; De Bari, C.; Dell'Accio, F.; Covelli, M.; Patella, V.; Lo Bianco, G.; Lapadula, G., Increased Expression of Nerve Growth Factor (NGF) and High Affinity NGF Receptor (p140 TrkA) in Human Osteoarthritic Chondrocytes. *Rheumatology (Oxford)* **2002,** *41* (12), 1413-8.
19. Huang, H.; Shank, G.; Ma, L.; Tallents, R. H.; Kyrkanides, S., Nerve Growth Factor Induced After Temporomandibular Joint Inflammation Decelerates Chondrocyte Differentiation. *Oral Dis* **2013,** *19* (6), 604-10.
20. Chuang, H. H.; Prescott, E. D.; Kong, H.; Shields, S.; Jordt, S. E.; Basbaum, A. I.; Chao, M. V.; Julius, D., Bradykinin and Nerve Growth Factor Release the Capsaicin Receptor from PtdIns(4,5)P2-mediated Inhibition. *Nature* **2001,** *411* (6840), 957-62.
21. Ji, R. R.; Samad, T. A.; Jin, S. X.; Schmoll, R.; Woolf, C. J., p38 MAPK Activation by NGF in Primary Sensory Neurons after Inflammation Increases TRPV1 Levels and Maintains Heat Hyperalgesia. *Neuron* **2002,** *36* (1), 57-68.
22. Schmelz, M.; Mantyh, P.; Malfait, A. M.; Farrar, J.; Yaksh, T.; Tive, L.; Viktrup, L., Nerve Growth Factor Antibody for the Treatment of Osteoarthritis Pain and Chronic Low-back Pain: Mechanism of Action in the Context of Efficacy and Safety. *Pain* **2019,** *160* (10), 2210-2220.
23. Nwosu, L. N.; Mapp, P. I.; Chapman, V.; Walsh, D. A., Blocking the Tropomyosin Receptor Kinase A (TrkA) Receptor Inhibits Pain Behaviour in Two Rat Models of Osteoarthritis. *Ann. Rheum. Dis.* **2015**.

24. Lane, N. E.; Schnitzer, T. J.; Birbara, C. A.; Mokhtarani, M.; Shelton, D. L.; Smith, M. D.; Brown, M. T., Tanezumab for the Treatment of Pain from Osteoarthritis of the Knee. *N. Engl. J. Med.* **2010,** *363* (16), 1521-31.
25. Xiao, S.; Tang, Y.; Lin, Y.; Lv, Z.; Chen, L., Tracking Osteoarthritis Progress through Cationic Nanoprobe-Enhanced Photoacoustic Imaging of Cartilage. *Acta Biomater* **2020,** *109*, 153-162.
26. Ye, J.; Li, Z.; Fu, Q.; Li, Q.; Zhang, X.; Su, L.; Yang, H.; Song, J., Quantitative Photoacoustic Diagnosis and Precise Treatment of Inflammation *In Vivo* Using Activatable Theranostic Nanoprobe. *Adv. Funct. Mater.* **2020,** *30* (38).
27. Xiao, S.; Chen, L., The Emerging Landscape of Nanotheranostic-based Diagnosis and Therapy for Osteoarthritis. *J Control Release* **2020,** *328*, 817-833.
28. Wang, L. V.; Hu, S., Photoacoustic Tomography: *In Vivo* Imaging from Organelles to Organs. *Science* **2012,** *335* (6075), 1458-62.
29. Choi, J.; Yang, J.; Jang, E.; Suh, J.S.; Huh, Y.M.; Lee, K.; Haam, S., Gold Nanostructures as Photothermal Therapy Agent for Cancer. *Anticancer Agents Med. Chem.* **2011**, *11*(10), 953-64.
30. Li, W.W.; Chen, X.Y. Gold Nanoparticles for Photoacoustic Imaging. *Nanomedicine* **2015**, *10*(2), 299-320.
31. Chen, Y. S.; Frey, W.; Kim, S.; Kruizinga, P.; Homan, K.; Emelianov, S., Silica-coated Gold Nanorods as Photoacoustic Signal Nanoamplifiers. *Nano Lett.* **2011,** *11* (2), 348-54.
32. Moon, H.; Kumar, D.; Kim, H.; Sim, C.; Chang, J. H.; Kim, J. M.; Kim, H.; Lim, D. K., Amplified Photoacoustic Performance and Enhanced Photothermal Stability of Reduced Graphene Oxide Coated Gold Nanorods for Sensitive Photoacoustic Imaging. *ACS Nano* **2015,** *9* (3), 2711-9.
33. Tian, F.; Lyu, J.; Shi, J.Y.; Yang M., Graphene and Graphene-like Two-denominational Materials based Fluorescence Resonance Energy Transfer (FRET) Assays for Biological Applications, *Biosens. Bioelectron.*, **2017**, *89* (1), 123-35,
34. Gupta, D.; Chauhan, V.; Kumar, R., A Comprehensive Review on Synthesis and Applications of Molybdenum Disulfide (MoS_2) Material: Past and Recent Developments. *Inorg. Chem. Commun.* **2020,** *108200.*
35. Oudeng, G.; Au, M.T.; Shi, J.Y.; Wen, C.Y.; Yang, M.**,** One-step in-situ Detection of MiRNA-21 Expression in Single Cancer Cells Based on Biofunctionalized MoS_2 Nanosheets, *ACS Appl. Mater. Interfaces*, **2018**,*10* (1), 350-360.
36. Shi, J.Y.; Lyu, J.; Tian, F.; Yang, M., A Fluorescence Turn-on Biosensor Based on Graphene Quantum Dots (GQDs) and Molybdenum Disulfide (MoS_2) Nanosheets for Epithelial Cell Adhesion Molecule (EpCAM) Detection, *Biosens. Bioelectron.* **2017**, *93*, 182–188.

37. Oudeng,G.; Benz, M.; Popova, A.; Zhang, Y.; Yi, C.Q.; Pavel, L.; Yang, M., Droplet-Microarray Based on Nanosensing Probe Patterns for Simultaneous Detection of Multiple HIV Retroviral Nucleic Acids, *ACS Appl. Mater. Interfaces,* **2020**, *12*(50), 55614–623.

38. Chou, S. S.; Kaehr, B.; Kim, J.; Foley, B. M.; De, M.; Hopkins, P. E.; Huang, J.; Brinker, C. J.; Dravid, V. P., Chemically Exfoliated MoS_2 as Near-infrared Photothermal Agents. *Angew. Chem. Int. Ed.* **2013,** *52* (15), 4160-4.

39. Chen, J.; Liu, C.; Hu, D.; Wang, F.; Wu, H.; Gong, X.; Liu, X.; Song, L.; Sheng, Z.; Zheng, H., Single-layer MoS_2 Nanosheets with Amplified Photoacoustic Effect for Highly Sensitive Photoacoustic Imaging of Orthotopic Brain Tumors. *Adv. Funct. Mater*. **2016,** *26* (47), 8715–8725.

40. Wang, S.; Li, X.; Chen, Y.; Cai, X.; Yao, H.; Gao, W.; Zheng, Y.; An, X.; Shi, J.; Chen, H., A Facile One-Pot Synthesis of a Two-Dimensional MoS2 /Bi2S3 Composite Theranostic Nanosystem for Multi-Modality Tumor Imaging and Therapy. *Adv Mater* **2015,** *27* (17), 2775-82.

41. Yu, J.; Yin, W.; Zheng, X.; Tian, G.; Zhang, X.; Bao, T.; Dong, X.; Wang, Z.; Gu, Z.; Ma, X.; Zhao, Y., Smart MoS2/Fe3O4 Nanotheranostic for Magnetically Targeted Photothermal Therapy Guided by Magnetic Resonance/Photoacoustic Imaging. *Theranostics* **2015,** *5* (9), 931-45.

42. Yossef Hay, O.; Cohen, M.; Nitzan, I.; Kasirer, Y.; Shahroor-Karni, S.; Yitzhaky, Y.; Engelberg, S.; Nitzan, M., Pulse Oximetry with Two Infrared Wavelengths without Calibration in Extracted Arterial Blood. *Sensors (Basel)* **2018,** *18* (10).

43. Nguyen, E. P.; Carey, B. J.; Ou, J. Z.; van Embden, J.; Gaspera, E. D.; Chrimes, A. F.; Spencer, M. J.; Zhuiykov, S.; Kalantar-Zadeh, K.; Daeneke, T., Electronic Tuning of 2D MoS_2 through Surface Functionalization. *Adv Mater* **2015,** *27* (40), 6225-9.

44. Glasson, S. S.; Blanchet, T. J.; Morris, E. A., The Surgical Destabilization of the Medial Meniscus (DMM) Model of Osteoarthritis in the 129/SvEv Mouse. *Osteoarthr. Cartil.* **2007,** *15* (9), 1061-1069.

45. Liu, Z.; Au, M.; Wang, X.; Chan, P.-M. B.; Lai, P.; Sun, L.; Zheng, Y.; Rong, L.; Wen, C., Photoacoustic Imaging of Synovial Tissue Hypoxia in Experimental Post-traumatic Osteoarthritis. *Prog. Biophys. Mol. Biol.* **2018**.

46. Robert P. Bonin; Bories, C.; Koninck, Y. D., A simplified Up-down Method (SUDO) for Measuring Mechanical Nociception in Rodents Using Von Frey Filaments. *Mol. Pain* **2014**.

For Table of Contents Only